Journal of Magnetism and Magnetic Materials 385 (2015) 198–206

Contents lists available at ScienceDirect

Journal of Magnetism and Magnetic Materials

journal homepage: www.elsevier.com/locate/jmmm

Control of wake and vortex shedding behind a porous circular obstacle by exerting an external magnetic field

M. Bovand [a], S. Rashidi [a,*], M. Dehghan [b], J.A. Esfahani [a], M.S. Valipour [b]

[a] Department of Mechanical Engineering, Ferdowsi University of Mashhad, P.O. Box 91775-1111, Mashhad, Iran
[b] Faculty of Mechanical Engineering, Semnan University, P.O. 35131-19111, Semnan, Iran

ARTICLE INFO

Article history:
Received 16 September 2014
Received in revised form
28 February 2015
Accepted 2 March 2015
Available online 3 March 2015

Keywords:
Vortex shedding
Porous bluff-body
Magnetic field
Finite volume method
Stuart number

ABSTRACT

In this article the finite volume method (FVM) is carried out to simulate the flow around and through a two-dimensional porous cylinder. An external magnetic field is used to control the wake behind the bluff body and also to suppress the vortex shedding phenomena. The Darcy–Brinkman–Forchheimer model has been used for modeling the flow in the porous medium. Effects of Stuart (N), Reynolds (Re) and Darcy (Da) numbers on the flow behavior have been investigated. The results show that the critical Stuart number for suppress vortex shedding decreases with increasing the Darcy numbers. Also, the Stuart number for disappearance the re-circulating wake increases with increased Reynolds number for both porous and solid cylinders.

1. Introduction

Investigation of the wake flow past bluff-bodies has received more attention in last two decades [45,37]. This type of study is vital in designing aeronautical, civil, mechanical, and chemical engineering platforms. Control of vortex shedding leads to a reduction in the unsteady forces acting on the bluff bodies and can significantly reduce their vibrations. When the drag is dominated by viscous drag, the body is called “streamlined”, and when it is dominated by pressure drag, the body is called “bluff”. Several kinds of control can be implemented to control bluff-body flows such as a modifying the geometry of surface (by putting tabs, streaks or dimples on the surface), blow and suction from body's surface, base bleed, controlling the boundary layer, etc. Some researchers utilized above techniques for controlling the wake and also suppressing vortex shedding. For example, control of vortex shedding in an axisymmetric bluff body wake by using a control disc was investigated by Weickgenannt and Monkewitz [48]. Mittal and Raghuvansh [25] carried out a study on control of vortex shedding hind circular cylinder for flows at low Reynolds numbers. In their study, the vortex shedding was controlled by a control cylinder. They found that the control cylinder provides a local favorable pressure gradient in the wake region thereby stabilizing the shear layer locally. Control of flow past a circular cylinder using small rotating cylinders was presented by Mittal [24]. It is observed that a significant reduction in the overall drag coefficient and the unsteady aerodynamic forces acting on the main cylinder is observed using this method. Also, control of vortex shedding on a circular cylinder using self-adaptive hairy-flaps was investigated by Kunze and Brucker [19]. The control of vortex shedding of a circular cylinder in shallow water using a splitter plate located in the downstream of the circular cylinder was investigated by Gozmen et al. [16]. Flow control around bluff bodies by attached permeable plates was studied by Ozkan and Akilli [31]. This study showed that attachment of angled permeable plates was effective on suppression of vortex shedding. Note that in all of the above researches, a secondary object has been used for control of wakes and suppression of vortex shedding. Some researchers control the wake flow by blow and suction from body's surface [22,14,26]. Also, some researchers used novel methods in order to achieve this objective. For example [21], investigated experimentally control of vortex shedding by thermal effect at low Reynolds numbers. They showed that this controlling method, easily realized by heating the bluff body, depends on the nature of the fluid. In another study, control of the near-wake flow around a circular cylinder with electro hydrodynamic actuators was studied by Artana et al. [1]. Their research established that the EHD actuator proposed was able to modify the flow in a large range of velocities. An experimental study was conducted to determine the effectiveness of the spanwise sinusoidal perturbation method (SPPM) in controlling vortex-induced vibrations by El-

* Corresponding author.
E-mail address: samanrashidi3983@gmail.com (S. Rashidi).

http://dx.doi.org/10.1016/j.jmmm.2015.03.012
0304-8853/

Nomenclature

B	uniform magnetic field strength (T)
C	a dimensionless coefficient (dimensionless)
D	cylinder diameter (m)
Da	Darcy number (dimensionless), $Da=K/D^2$
F	force (N)
J	electrical current density (A/m^2)
K	permeability (m^2)
L	length (m)
N	Stuart number (dimensionless), $N=\sigma B^2 D/(\rho U_\infty)$
p	pressure (Pa)
r	radial coordinate (m)
R	cylinder radius (m)
Re	Reynolds number (dimensionless), $\rho U_\infty D/\mu$
t	time (s)
u, v	velocity component in r *and* θ direction respectively (ms^{-1})
V	velocity vector (ms^{-1})

Greek symbols

μ	dynamic viscosity (kg m^{-1} s^{-1})
υ	fluid kinematic viscosity (m^2 s^{-1}), $\upsilon=\mu/\rho$
ρ	fluid density (kg m^{-3})
ε	porosity (dimensionless)
θ	cross-radial coordinate (dimensionless)
σ	electrical conductivity of the fluid (1/Ωm)
ω	vorticity (s^{-1})
β_1, β_2	stress jump parameters

Subscripts/superscripts

c	particle
cr	critical
d,D	drag
dis	disappearance
F	Forchheimer
p	pressure
R	recirculating
υ	viscous
∞	free stream
1	clear fluid domain
2	porous domain
$*$	dimensional variables

Gammal et al. [11]. Fu and Rockwell [15] delayed the vortex formation in the near wake of shallow flow past a vertical cylinder by base bleed through a very narrow slot.

An experimental investigation on the use of plasma actuators for vortex shedding suppression was performed by Nati et al. [27]. It was found that the total kinetic energy contained in the fluctuating components of the velocity field is reduced by approximately 60% compared to the case without plasma actuation.

In recent years, an increasing attention is given to the MHD flows [42–44]. Yoon et al. [50] presented the results of a numerical study on the fluid flow and heat transfer parameters around a circular cylinder in the presence of a magnetic field. Yoon et al. [17] studied steady and unsteady MHD flows past a cylinder with circular cross section utilizing the immersed boundary method. Valipour et al. [46] investigated Magnetohydrodynamics flow and heat transfer around a solid cylinder wrapped with a porous ring.

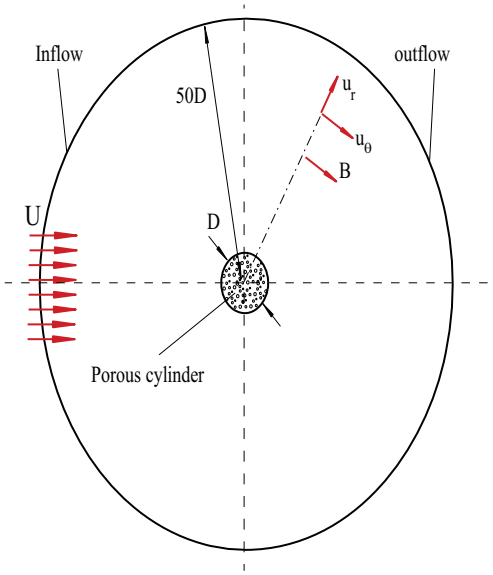

Fig. 1. Geometrical description of the computational domain.

They used the least square method [34,35,18] and presented two equations for the average Nusselt number.

Control of wake and vortex shedding of flow past a bluff-body have been widely studied by researchers in the past decades. In this study, two methods are presented for controlling the alternating wake patterns of flow past the cylinders. These are; exerting an external magnetic field and manipulation in the porous material structure.

This paper presents the results of a numerical study of fluid flow around a porous circular cylinder in the existence of a cross-radial magnetic field. It presents the effect of a cross-radial magnetic field on several hydrodynamics parameters, such as the drag coefficient, the length of the recirculation region, the streamlines and vorticity in the laminar regime at moderate Re numbers.

2. Mathematical formulation

2.1. Problem description

The system of interest is a two-dimensional porous circular cylinder with diameter "D". An incompressible fluid of density "ρ", molecular viscosity "μ" is considered. Uniform flow with velocity "U_∞" flows around and through a very long porous circular cylinder. The computational domain is presented schematically in Fig. 1. In this study following assumptions are made [5,6,39,40,8,9,10]:

- Two-dimensional, steady, laminar flow of an incompressible and viscous flow has been considered.
- The porous structure is uniform and homogeneous.
- The porous cylinder is fully saturated with the working fluid.
- Two-domain approach is used for pertinent governing equations.
- The diameter of porous cylinder is sufficiently larger than the characteristics radius of the medium's pores and satisfies the volume-averaged equations used in this study.
- The intensity of magnetic field around the cylinder "B" varies with respect to r like as

$$\vec{B} = B_0 \frac{R}{r} e_\theta \tag{1}$$

where B_0 and R are the intensity of the magnetic field on the cylinder and the cylinder radius, respectively. Note that, the magnetic field has to obey two pertinent laws. The first is that the field has to be solenoidal, that is $\nabla \cdot$ B= 0. This requirement is met in this study. The second is Ampere's law. In this paper, there is no applied current density and so Ampere's law reduces to the requirement that the field is irrotational, that is that $\nabla \times$ B= 0. In terms of cylindrical polar coordinates (r, θ, z), we assume a magnetic field B=(0, B_0/r, 0), and so $\nabla \times B = (-\partial B/\partial z,\ 0,\ 1/r\partial(rB)/\partial r) = 0$

2.2. Governing equations

As mentioned in the previous section, two-domain approach is used for pertinent governing equations in this study. Therefore the governing equations must be solved for two zones, the clear fluid zone and the porous medium one. Hence, two sets of equations were considered here, one set for the clear domain that are indicated by subscript 1, and a second set for the porous layer denoted by subscript 2. The governing equations are made dimensionless by using the following dimensionless variables [36]:

$$r = \frac{r^*}{R},\ \theta = \theta^*,\ u = \frac{u^*}{U_\infty},\ v = \frac{v^*}{U_\infty},\ p = \frac{p^*}{\rho U_\infty^2} \tag{2}$$

where superscript "*" denotes dimensional variables.

2.2.1. Governing equations for the clear domain

Mass conservation equation is

$$\frac{\partial}{\partial r}(ru_1) + \frac{\partial}{\partial \theta}(v_1) = 0 \tag{3}$$

The momentum equations in the r and θ directions are

$$\frac{\partial u_1}{\partial t} + \frac{v_1}{r}\frac{\partial u_1}{\partial \theta} + u_1\frac{\partial u_1}{\partial r} - \frac{v_1^2}{r} = -\frac{\partial p_1}{\partial r} + \frac{2}{\mathrm{Re}}\left(\frac{\partial^2 u_1}{\partial r^2} + \frac{1}{r}\frac{\partial u_1}{\partial r} + \frac{1}{r^2}\frac{\partial^2 u_1}{\partial \theta^2} - \frac{2}{r^2}\frac{\partial v_1}{\partial \theta} - \frac{u_1}{r^2}\right) - \underbrace{\frac{u_1 N}{2}}_{MHD\ term} \tag{4}$$

$$\frac{\partial v_1}{\partial t} + \frac{v_1}{r}\frac{\partial v_1}{\partial \theta} + u_1\frac{\partial v_1}{\partial r} + \frac{u_1 v_1}{r} = -\frac{1}{r}\frac{\partial p_1}{\partial \theta} + \frac{2}{\mathrm{Re}}\left(\frac{\partial^2 v_1}{\partial r^2} + \frac{1}{r}\frac{\partial v_1}{\partial r} + \frac{1}{r^2}\frac{\partial^2 v_1}{\partial \theta^2} + \frac{2}{r^2}\frac{\partial u_1}{\partial \theta} - \frac{v_1}{r^2}\right) \tag{5}$$

2.2.2. Governing equations for the porous layer

Mass conservation equation in the porous region is

$$\frac{\partial}{\partial r}(ru_2) + \frac{\partial}{\partial \theta}(v_2) = 0 \tag{6}$$

The momentum equations in the r and θ directions in the porous region are

$$\frac{1}{\varepsilon^2}\left(\varepsilon\frac{\partial u_2}{\partial t} + \frac{v_2}{r}\frac{\partial u_2}{\partial \theta} + u_2\frac{\partial u_2}{\partial r} - \frac{v_2^2}{r}\right) = -\frac{\partial p_2}{\partial r} + \underbrace{\frac{2}{\varepsilon Re}\left(\frac{\partial^2 u_2}{\partial r^2} + \frac{1}{r}\frac{\partial u_2}{\partial r} + \frac{1}{r^2}\frac{\partial^2 u_2}{\partial \theta^2} - \frac{2}{r^2}\frac{\partial v_2}{\partial \theta} - \frac{u_2}{r^2}\right)}_{Brinkmanterm} - \underbrace{\frac{1}{2ReDa}u_2}_{Darcyterm} - \underbrace{\frac{C_F}{2\sqrt{Da}}\sqrt{u_2^2 + v_2^2}\,u_2}_{Forchheimerterm} - \underbrace{\frac{u_2 N}{2}}_{MHDterm} \tag{7}$$

$$\frac{1}{\varepsilon^2}\left(\varepsilon\frac{\partial v_2}{\partial t} + \frac{v_2}{r}\frac{\partial v_2}{\partial \theta} + u_2\frac{\partial v_2}{\partial r} + \frac{u_2 v_2}{r}\right) = -\frac{1}{r}\frac{\partial p_2}{\partial \theta} + \underbrace{\frac{2}{\varepsilon Re}\left(\frac{\partial^2 v_2}{\partial r^2} + \frac{1}{r}\frac{\partial v_2}{\partial r} + \frac{1}{r^2}\frac{\partial^2 v_2}{\partial \theta^2} + \frac{2}{r^2}\frac{\partial u_2}{\partial \theta} - \frac{v_2}{r^2}\right)}_{Brinkmanterm} - \underbrace{\frac{1}{2ReDa}v_2}_{Darcyterm} - \underbrace{\frac{C_F}{2\sqrt{Da}}\sqrt{u_2^2 + v_2^2}\,v_2}_{Forchheimerterm} \tag{8}$$

where Da and Re are the Darcy number and Reynolds number, respectively, defined by

$$Da = \frac{K}{D^2},\ Re = \frac{\rho U_\infty D}{\mu} \tag{9}$$

N is called the Stuart or the interaction parameter, which is the ratio of the electromagnetic force to the inertial force, expressed as [50]

$$N = \frac{\sigma B^2 D}{\rho U_\infty} \tag{10}$$

The volume-averaged fluid velocity $\vec{V}$ inside the porous layer with porosity ε is related to the Darcy velocity $\vec{v}$ through Dupuit–Forchheimer relationship, as $\vec{v} = \varepsilon\vec{V}$. The Forchheimer coefficient, C_F, is defined by [12]

$$C_F = \frac{1.75}{\sqrt{150\varepsilon^3}} \tag{11}$$

2.3. The boundary conditions

To minimize the effect of the outer boundaries, the dimensions of the computational domain were defined as being fifty times larger than the diameter of the cylinder [47]. The governing equations, Eqs. (3)–(8), are subjected to the following boundary conditions:

Along the upstream boundary (uniform flow):

$$u_1 = -\cos\theta,\ v_1 = \sin\theta \tag{12}$$

Along the downstream boundary:

$$\frac{\partial u_1}{\partial r} = 0,\ \frac{\partial v_1}{\partial r} = 0 \tag{13}$$

For the interface between the porous and the fluid regions, continuity of the velocity and the stress-jump condition for shear stress are used. In the stress-jump condition the stress in the fluid is not continuous across the clear-fluid and the porous-medium interface. Ochoa-Tapia and Whitaker [29] and Ochoa-Tapia et al. [30] used the sophisticated volume averaging method to develop a jump boundary condition at the interface based on the modified Brinkman equation as the governing equation. These conditions at the porous–fluid interface are as following:

$$u_1 = u_2 \tag{14}$$

$$v_1 = v_2 \tag{15}$$

$$\frac{\mu_f}{\varepsilon}\frac{\partial v_2}{\partial r} - \mu_f \frac{\partial v_1}{\partial r} = \beta_1 \frac{\mu}{\sqrt{k}} v|\text{interface} + \beta_2 \rho v^2|\text{interface} \tag{16}$$

where β_1 and β_2 are adjustable parameters which account for the stress jump at the interface.

The first coefficient β_1 has a more noticeable effect whereas the second coefficient β_2 has small effect [2]. Note that Rashidi et al. [41] have shown that this boundary condition is general that both the viscous and the inertial effects are considered in it. Thus, in the present simulation β_1 and β_2 have been chosen 0.7 [41]. Also, the initial conditions are assumed to be a uniform incoming flow.

2.4. Numerical method

In the present simulation, Finite-Volume Method (FVM) is used to numerically solve the governing Eqs. (1) and (2) along with the relevant boundary conditions. Staggered grid system is used where the velocity components are stored at cell faces and pressure is stored at the cell center. To speed up the simulation, a non-uniform structured grid system is used [3,23,4,7]. The SIMPLE algorithm [33] is utilized for pressure–velocity de-coupling and iteration. The first order implicit scheme has been employed to discretize the time derivatives and a third-order accurate QUICK scheme (Quadratic Upwind Interpolation for Convective Kinematics) for the convective referenced [33]. The convergence is assumed to be achieved when the summation of residuals decreased to $\leq 10^{-7}$ for all equations. The numerical simulation was used to find the flow behavior, velocity distribution, drag coefficient and streamlines.

2.5. Grids-independent study

Fig. 2 shows a sample of grid distribution along the r- and θ-directions near the interface of porous cylinder and the fluid region. The whole computational domain is divided into three subdomains, A, B and C. In this category, C is for clear fluid zone, and A and B are for the porous domain. As it can be seen, the O-grid type method is used for mesh generation inside the porous cylinder. For

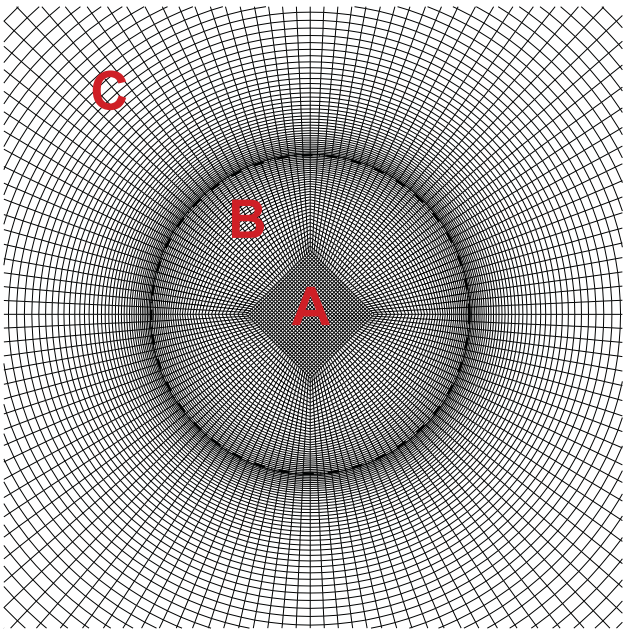

Fig. 2. A typical example of grid near the cylinder (A: 70×70; B: 280×70; C: 280×200).

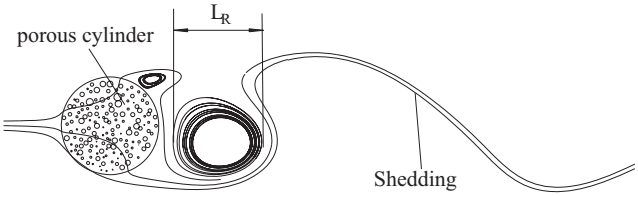

Fig. 3. Geometrical parameters of the recirculating wake.

obtain fine grid, the grid in the radial direction were stretched with dense grid in r-direction with $\delta r=0.002$ near the porous–fluid interface. It is examined to ensure a grid-independent solution. The test is performed for three different grid sizes for both porous and solid circular cylinder regions at $Re=100$, $N=0$, $Da=5\times10^{-3}$.

Geometrical parameters of the wake are available in Fig. 3. Table 1 summarizes the comparisons of drag coefficient for various grid sizes. For the solid and porous cylinder, the differences in C_D between cases 2 and 3 are 0.40% and 0.30% respectively. Therefore, the grid of case 3 is chosen for the final simulations.

2.6. Validation

In this section, in order to demonstrate the validity of the numerical simulation we compare the variation of wake length for the solid cylinder, at different Reynolds numbers with the results of Park et al. [32] and Fornberg [13]. As can be seen in Fig. 4, the results are in a good agreement. Also, for comparison the results are shown for porous cylinder in this figure. As it can be seen in this figure, the wake length becomes smaller with an increase in the Reynolds number and this reduction is sensible for $Re<80$. By comparing the results shown in this figure, it can be seen that at small Darcy numbers (for example $Da=10^{-15}$), the flow pattern around a porous cylinder is similar to a solid cylinder. For small Darcy numbers, the flow resistance is high, which means fluid can hardly penetrate into the porous region [38].

3. Results and discussion

In this study, the fluid flow is governed by the physical parameters, such as the Darcy, Reynolds, and Stuart numbers. This problem is analyzed for different values of Reynolds number, $1<Re<200$ and Darcy number, $10^{-6}<Da<10^{-2}$ and Stuart number, $0<N<10$. The porosity (ε) is considered to be 0.7 for all cases. Fig. 5 shows the variation of wake length with Darcy numbers at $Re=100$ and $N=0$. Note that in this paper, $N=0$ represents the absence of an external magnetic field. It can be

Table 1
Effect of grid size on C_D and L_R; $Re=100$, $N=0$, $Da=5\times10^{-3}$.

Case	Grid size			C_D	*Percentage difference (%)*
	Domain A	Domain B	Domain C		
Solid cylinder					
1	–	–	120×100	1.324	0.9
2	–	–	240×160	1.336	0.3
3	–	–	360×220	1.34	–
Porous cylinder					
1	20×20	120×15	120×100	1.093	1.1
2	30×30	240×30	240×160	1.1055	0.4
3	40×40	360×45	360×220	1.11	–

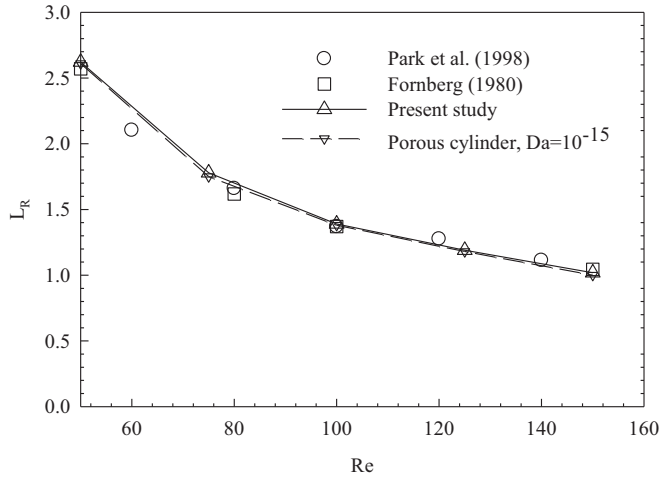

Fig. 4. Variation of the wake length with Reynolds number.

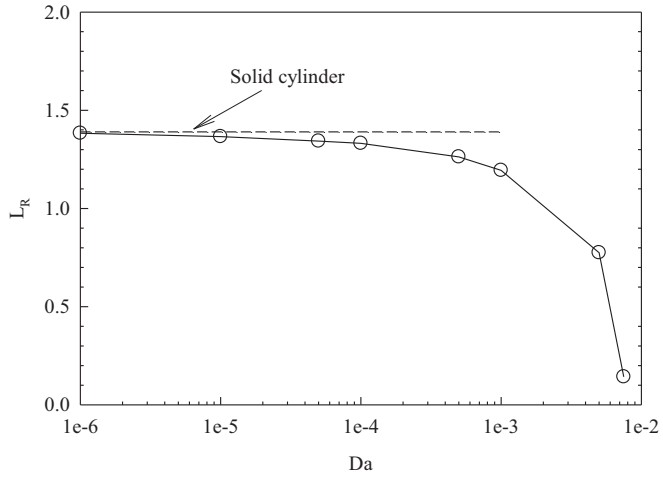

Fig. 5. Variation of the wake length with Darcy numbers ($Re=100$, $N=0$).

observed that the wake length decreases with increasing Darcy number because the separation is delayed with an increase in the Darcy number [38]. Also this figure shows that the porous cylinder approaches the corresponding case of a solid cylinder for low Darcy numbers, typically at Darcy numbers lower than 10^{-6}.

The streamline and vorticity contours for different Darcy numbers and at $Re=100$ and $N=0$ are displayed in Fig. 6. As shown in this figure, the flow is time-dependent and we can observe that large vortices are shed periodically behind the body of a solid cylinder. For a porous cylinder, the boundary layer thickness increases on the cylinder surface and the vortex street in the wake region is elongated in the streamwise direction with decreasing vortex strength. The flow is still time-dependent at $Da=5\times10^{-3}$. If the Darcy number is increased further to 1×10^{-2}, the flow is stabilized and it changes the distribution from the time-dependent pattern with vortex shedding in the wake to the steady-state one with asymmetric shape along the centerline. The base-bleed effect (secondary flow that is injected at the base of the truncated plug [20] and external flow are the main reasons for these changes from the time-dependent pattern to the steady-state one. Therefore, one way to suppress the vortex shedding of a cylinder is by controlling the permeability of the porous material. Note that vortex shedding creates an unsteady, periodic force which makes the bluff body vibrate and may lead to structural failure and consequently this is critical to suppress vortex shedding.

Streamline and vorticity contours for solid and porous cylinders at different Stuart number and $Re=100$ are shown in Figs. 7 and 8, respectively. As shown in Eqs. (4) and (7), if the magnetic field is applied in the cross-radial direction, the radial force acts in the negative r-direction and this tends to retard the motion of the fluid. This resistive force is called as the Lorentz force which experienced by a fluid carrying a current density J in a magnetic field B and calculates as follow:

$$\vec{F}_{Lorentz}=\vec{J}\times\vec{B}=\sigma(\vec{V}\times\vec{B})\times B \tag{17}$$

This figure shows that if the Stuart number increases, the flow is stabilized and the distribution changes from the time-dependent pattern to the steady-state one. The flow is steady for $N=0.22$ for solid cylinder. However, if N is further increased to 5, the re-

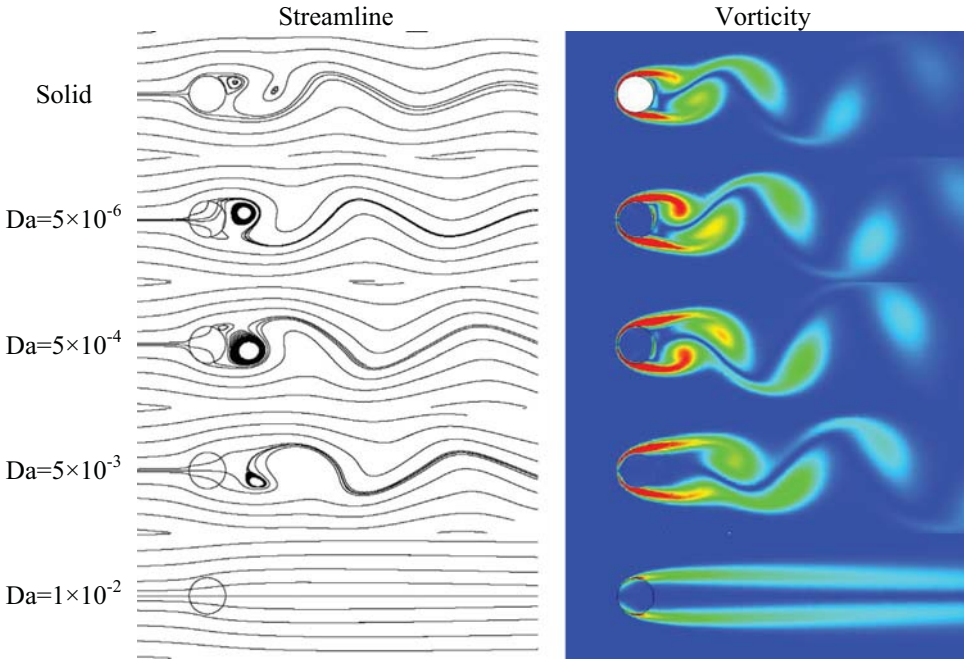

Fig. 6. Contours of streamline and vorticity for different Darcy numbers ($N=0$, $Re=100$).

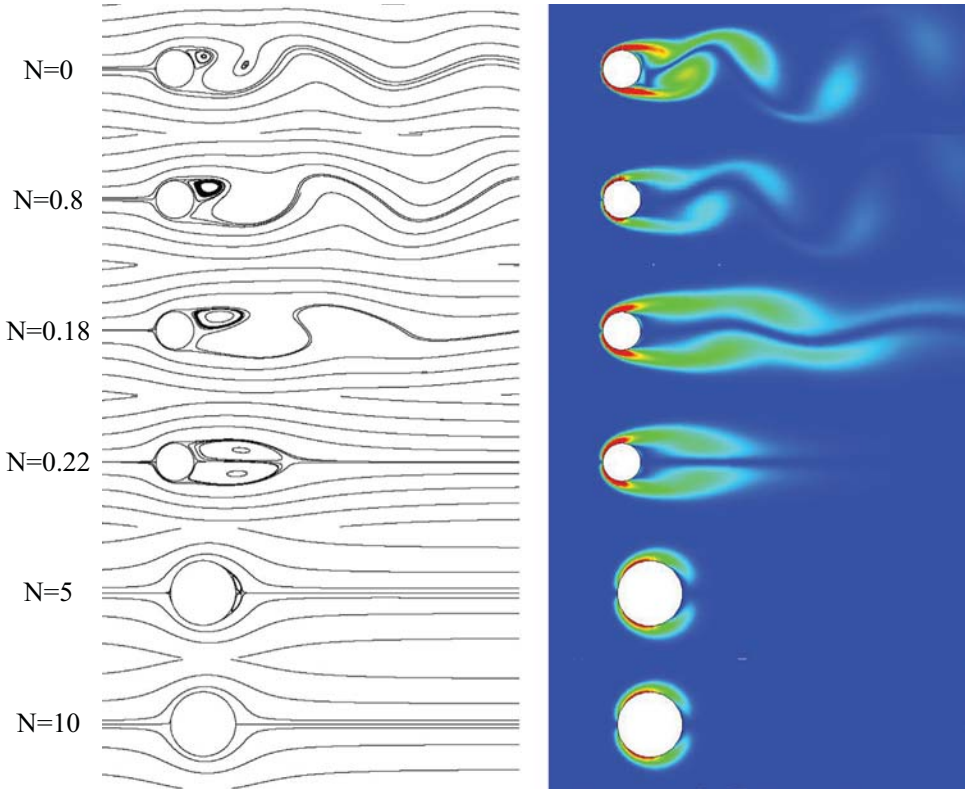

Fig. 7. Contours of streamline and vorticity for solid cylinder at different Stuart numbers ($Re=100$).

circulating wake weakens and it completely disappears when the Stuart number reaches 10. Note that it is pointed out that magnetic field effects are often negligible in porous media [28]; however, this argument is correct for the cases where the entire computation domain is in the porous media. In our problem, the majority of domain is not porous. Therefore, the magnetic field can affect the flow pattern by altering the working fluid velocity distribution in the clear fluid region. Moreover, by comparing the results shown in Figs. 7 and 8, we can conclude that the suppressing of the vortex shedding is occurred by smaller magnetic field strength for a porous cylinder.

Fig. 9 shows the variation of the drag coefficient with respect to the Stuart number at different Darcy numbers and $Re=100$. Drag coefficient is defined as follows [49]:

$$C_D = C_{D_v} + C_{D_p} = \frac{F_d}{1/2\rho U_\infty^2 D} \tag{18}$$

Here, subscripts p and v denotes the pressure and viscous

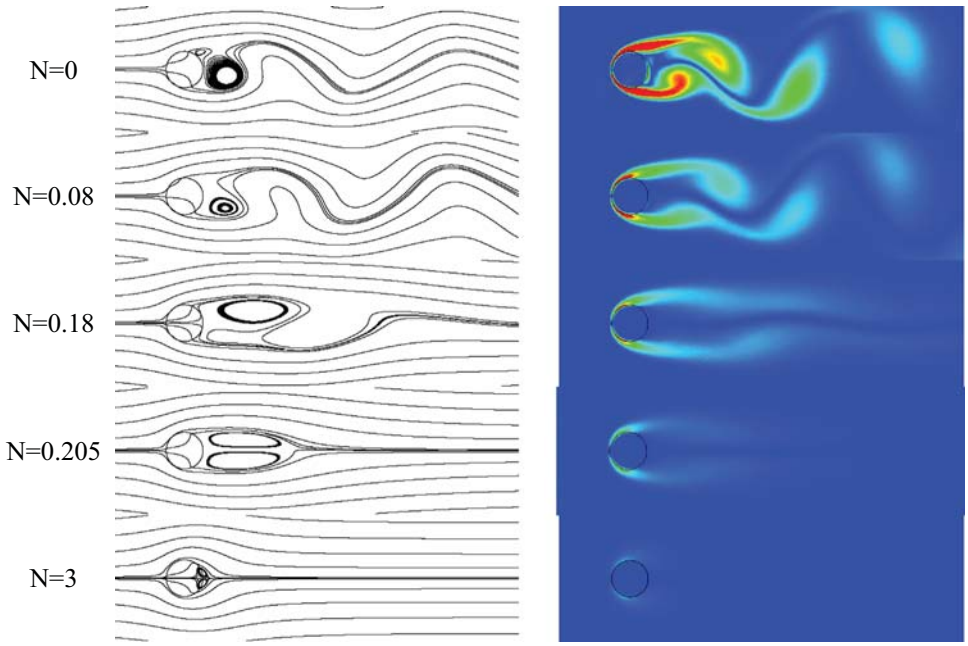

Fig. 8. Contours of streamline and vorticity for porous cylinder at different Stuart numbers ($Da=5\times10^{-4}$, $Re=100$).

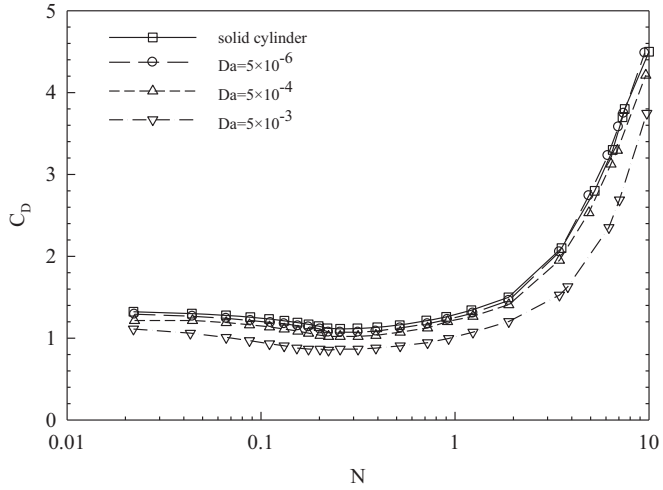

Fig. 9. Variation of drag coefficient with Stuart numbers at different Darcy numbers ($Re=100$).

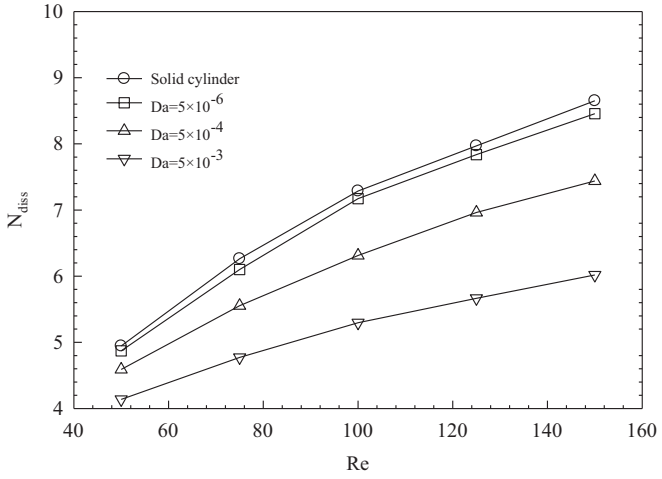

Fig. 11. Variation of the disappearance Stuart number with Reynolds numbers at different Darcy numbers.

forces, respectively. The drag force per unit length on the cylinder is calculated as [51]

$$F_d = \frac{DU_\infty}{2}\int_0^{2\pi}(-p\rho U_\infty \cos\theta - 2\nu\omega \sin\theta)d\theta \tag{19}$$

This figure shows that drag coefficient decreases slowly and then increases rapidly with increasing Stuart number. In general, by exerting a magnetic field, the Lorentz force is acting directly to dump the velocity component. Also, increasing in the magnetic field strength leads to an increase in the difference between the upstream and downstream pressures, and an increase in the drag coefficients. The drag reduction for weak magnetic fields is due to the distribution of the pressure forces around the cylinder. It is worth mentioning that this reduction is continued until Stuart number equal to 0.22 and as mentioned in description of previous figure, in this Stuart number the flow is stabilized and the time-dependency vanishes.

It is also observed that the drag coefficient decreases with increasing Darcy number because a highly permeable cylinder allows the fluid to flow through it with the least resistance and this resistance increases as the Darcy number decreases. It is worth mentioning that for small Darcy numbers, the drag coefficient approaches an asymptote which equals to that of a solid cylinder.

Fig. 10 shows the critical Stuart number variation as a function of the Reynolds number at different Darcy numbers. Here N_{cr} is a value of the Stuart number, at which the flow pattern changes from the time-dependent pattern to the steady-state one. This critical number depends on the Reynolds and Darcy numbers. It is observed that the critical Stuart number increases with increasing Reynolds number for all Darcy numbers but this augmentation is slowly for $Da=8.3\times10^{-3}$. It is also observed that the critical Stuart number decreases with increasing Darcy number. This reduction is much clear between the cases of $Da=5\times10^{-3}$ and $Da=8.3\times10^{-3}$, because for higher Darcy numbers, the control of wake and vortex shedding is performed mostly by base bleed effect rather than the external magnetic field effects. Therefore, it is worth mentioning that for small Darcy numbers, the control of wake and vortex shedding is performed mostly by the external magnetic field.

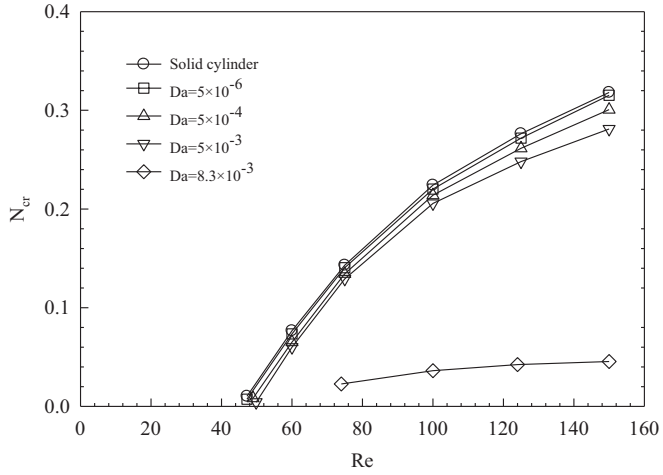

Fig. 10. Variation of the critical Stuart number with Reynolds numbers at different Darcy numbers.

The disappearance Stuart number is plotted against Reynolds number with Darcy number as a parameter in Fig. 11.The disappearance Stuart number N_{dis}, is defined to measure the strength of the inserted magnetic field required for disappearing the recirculating wake. It is found that the disappearance Stuart number increases with Reynolds number for both porous and solid cylinders. Also, the value of disappearance Stuart number decreases when Darcy number increases. Note that bluff bodies experience pressure drag due to the existence of a large wake and so it is critical to control of this wake.

Effect of the magnetic field strength on the time evolution of the drag coefficient is shown in Fig. 12. The dashed line denotes the activation of the magnetic field at $t=150$. In this figure blue line refers to solid cylinder and red line refers to porous cylinder. This figure shows that for weak magnetic fields, ($N<0.22$), drag coefficient decreases by exerting magnetic field. Within this range, the shear stress forces were found to decrease monotonically with N. It is interesting to note that fluctuations in drag coefficient are reduced by exerting magnetic field and the diagrams have a monotonic behavior. Also, for strong magnetic fields, (i.e. $N=5$), drag coefficient increases by exerting magnetic field. Note that the drag coefficient for a porous cylinder is less than a solid cylinder.

4. Conclusion

A numerical study has been carried out to study the effect of magnetic field and porous material properties in controlling the wake formation and suppressing the vortex shedding. This problem is a classical problem with great challenges in fluid

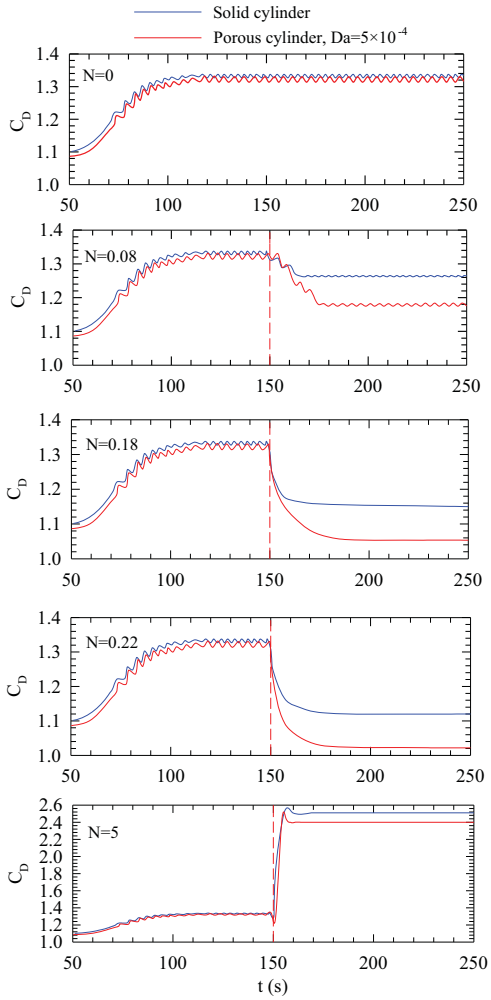

Fig. 12. Variation of drag coefficient with time at different Stuart numbers for solid and porous cylinders. (For interpretation of the references to color in this figure, the reader is referred to the web version of this article.)

mechanics. The most important obtained results are highlighted as follows:

- The wake length decreases with increasing the Darcy numbers.
- If the Darcy number is increased, the flow is stabilized and distribution changes from the time-dependent pattern with vortex shedding in the wake to the steady-state one with asymmetric shape along the centerline.
- For small Darcy numbers, the drag coefficient approaches an asymptote which equals to that of a solid cylinder.
- Critical Stuart number for suppressing the vortex shedding decreases with increasing the Darcy numbers.
- For small Darcy numbers, the control of wake and vortex shedding is performed mostly due to the external magnetic field.
- The value of disappearance Stuart number decreases when the Darcy number increases.

References

[1] G. Artana, R. Sosa, E. Moreau, G. Touchard, Control of the near-wake flow around a circular cylinder with electrohydrodynamic actuators, Exp. Fluids 35 (2003) 580–588.
[2] X. Chen, P. Yu, S.H. Winoto, H.-T. Low, Numerical analysis for the flow past a porous square cylinder based on the stress-jump interfacial-conditions, Int. J. Numer. Methods Heat Fluid Flow 18 (2008) 635–655.
[3] M. Dehghan, H. Basirat Tabrizi, On near-wall behavior of particles in a dilute turbulent gas–solid flow using kinetic theory of granular flows, Powder Technol. 224 (2012) 273–280.
[4] M. Dehghan, H. Basirat Tabrizi, Turbulence effects on the granular model of particle motion in a boundary layer flow, Can. J. Chem. Eng. 92 (2014) 189–195.
[5] M. Dehghan, M. Tajik Jamal-Abad, S. Rashidi, Analytical interpretation of the local thermal non-equilibrium condition of porous media imbedded in tube heat exchangers, Energy Convers. Manag. 85 (2014) 264–271.
[6] M. Dehghan, M.S. Valipour, S. Saedodin, Perturbation analysis of the local thermal non-equilibrium condition in a fluid saturated porous medium bounded by an iso-thermal channel, Transp. Porous Media 102 (2014) 139–152.
[7] M. Dehghan, M. Daneshipour, M.S. Valipour, R. Rafee, S. Saedodin, Enhancing heat transfer in microchannel heat sinks using converging flow passages, Energy Convers. Manag. 92 (2015) 244–250.
[8] M. Dehghan, Y. Mahmoudi, M.S. Valipour, S. Saedodin, Combined conduction-convection-radiation heat transfer of slip flow inside a micro-channel filled with a porous material, Transp. Porous Media (2015) (in preparation).
[9] M. Dehghan, Y. Rahmani, D.D. Ganji, S. Saedodin, M.S. Valipour, S. Rashidi, Convection-radiation heat transfer in solar heat exchangers filled with a porous medium: homotopy perturbation method versus numerical analysis, Renew. Energy 74 (2015) 448–455.
[10] M. Dehghan, M.S. Valipour, S. Saedodin, Temperature-dependent conductivity in forced convection of heat exchangers filled with porous media: a perturbation solution, Energy Convers. Manag. 91 (2015) 259–266.
[11] M. El-Gammal, H. Hangan, P. King, Control of vortex shedding-induced effects in a sectional bridge model by spanwise perturbation method, J. Wind Eng. Ind. Aerodyn. 95 (2007) 663–678.
[12] P.H. Forchheimer, Z. Ver. Dtsch. Ing. 45 (1901) 1782–1788.
[13] B. Fornberg, A numerical study of steady viscous flow past a circular cylinder, J. Fluid Mech. 98 (1980) 819–855.
[14] J.H.M. Fransson, P. Konieczny, P.H. Alfredsson, Flow around a porous cylinder subject to continuous suction or blowing, J. Fluids Struct. 19 (8) (2004) 1031–1048.
[15] H. Fu, D. Rockwell, Shallow flow past a cylinder: control of the near wake, J. Fluid Mech. 539 (2005) 1–24.
[16] B. Gozmen, H. Akilli, B. Sahin, Passive control of circular cylinder wake in shallow flow, Measurement 46 (2013) 1125–1136.
[17] D.G.E. Grigoriadis, I.E. Sarris, S.C. Kassinos, MHD flow past a circular cylinder using the immersed boundary method, Comput. Fluids 39 (2010) 345–358.
[18] F. Jazebi, A. Rashidi, An automated procedure for selecting project managers in construction firms, J. Civ. Eng. Manag. 19 (1) (2013) 97–106.
[19] S. Kunze, C. Brucker, Control of vortex shedding on a circular cylinder using self-adaptive hairy-flaps, C. R. Méc. 340 (2012) 41–56 (1–2).
[20] L.G. Leal, A. Acrivos, The effect of base bleed on the steady separated flow past bluff objects, J. Fluid Mech. 39 (1970) 735–752.
[21] J.-C. Lecordier, L.W.B. Browne, S. Le Masson, F. Dumouchel, P. Paranthoen, Control of vortex shedding by thermal effect at low Reynolds numbers, Exp. Therm. Fluid Sci. 21 (2000) 227–237.
[22] Z. Li, I.M. Navon, M.Y. Hussaini, F.-X. Le Dimet, Optimal control of cylinder wakes via suction and blowing, Comput. Fluids 32 (2003) 149–171.
[23] M. Mirzaei, M. Dehghan, Investigation of flow and heat transfer of nanofluid in microchannel with variable property approach, Heat Mass Transf. 49 (2013) 1803–1811.
[24] S. Mittal, Control of flow past bluff bodies using rotating control cylinders, J. Fluids Struct. 15 (2001) 291–326.
[25] S. Mittal, A. Raghuvanshi, Control of vortex shedding behind circular cylinder for flows at low Reynolds numbers, Int. J. Numer. Methods Fluids 35 (2001) 421–447.
[26] K. Muralidharan, S. Muddada, B.S.V. Patnaik, Numerical simulation of vortex induced vibrations and its control by suction and blowing, Appl. Math. Model. 37 (2013) 284–307 (1–2).
[27] G. Nati, M. Kotsonis, S. Ghaemi, F. Scarano, Control of vortex shedding from a blunt trailing edge using plasma actuators, Exp. Therm. Fluid Sci. 46 (2013) 199–210.
[28] D.A. Nield, Impracticality of MHD convection in a porous medium, Transp. Porous Media 73 (2008) 379–380.
[29] J.A. Ochoa-Tapia, S. Whitaker, Momentum transfer at the boundary between a porous medium and a homogeneous fluid I: theoretical development, Int. J. Heat Mass Transf. 38 (1995) 2635–2646.
[30] J.A. Ochoa-Tapia, S. Whitaker, Momentum transfer at the boundary between a porous medium and a homogeneous fluid II: comparison with experiment, Int. J. Heat Mass Transf. 38 (1995) 2647–2655.
[31] G.M. Ozkan, H. Akilli, Flow control around bluff bodies by attached permeable plates, Int. J. Mech. Aerosp. Ind. Mechatron. Eng. 8 (5) (2014) 1035–1039.
[32] J. Park, K. Kwon, H. Choi, Numerical solutions of flow past a circular cylinder at Reynolds number up to 160, KSME Int. J. 12 (6) (1998) 1200–1205.
[33] S.V. Patankar, Numerical Heat Transfer and Fluid Flow, Hemisphere, New York, 1980.
[34] A. Rashidi, H. Fathi, I. Brilakis, Innovative stereo vision-based approach to generate dense depth map of transportation infrastructure, Transp. Res. Rec. J. Transp. Res. Board 2215 (2011) 93–99.
[35] A. Rashidi, H. Rashidi-Nejad, M. Maghiar, Productivity estimation of bulldozers

using generalized linear mixed models, KSCE J. Civ. Eng. 18 (6) (2014) 1580–1589.
[36] S. Rashidi, A. Tamayol, M.S. Valipour, N. Shokri, Fluid flow and forced convection heat transfer around a solid cylinder wrapped with a porous ring, Int. J. Heat Mass Transf. 63 (2013) 91–100.
[37] S. Rashidi, R. Masoodi, M. Bovand, M.S. Valipour, Numerical study of flow around and through a porous diamond cylinder with different apex angels, Int. J. Numer. Methods Heat Fluid Flow 24 (7) (2014) 1504–1518.
[38] S. Rashidi, M. Bovand, I. Pop, M.S. Valipour, Numerical simulation of forced convective heat transfer past a square diamond-shaped porous cylinder, Transp. Porous Media 102 (2) (2014) 207–225.
[39] S. Rashidi, M. Dehghan, R. Ellahi, M. Riaz, M.T. Jamal-Abad, Study of stream wise transverse magnetic fluid flow with heat transfer around an obstacle embedded in a porous medium, J. Magn. Magn. Mater. 378 (2015) 128–137.
[40] S. Rashidi, M. Bovand, J.A. Esfahani, H.F. Öztop, R. Masoodi, Control of wake structure behind a square cylinder by magnetohydrodynamics, ASME J. Fluids Eng. (2015), http://dx.doi.org/10.1115/1.4029633.
[41] S. Rashidi, A. Nouri-Borujerdi, M.S. Valipour, R. Ellahi, I. Pop, Stress-jump and continuity interface conditions for a cylinder embedded in a porous medium, Transp. Porous Media 107 (1) (2015) 171–186.
[42] M. Sheikholeslami, M. Gorji Bandpy, R. Ellahi, A. Zeeshan, Simulation of MHD CuO–water nanofluid flow and convective heat transfer considering Lorentz forces, J. Magn. Magn. Mater. 369 (2014) 69–80.
[43] M. Sheikholeslami, M. GorjiBandpy, M. Younus Javed, R. Ellahi, Effect of thermal radiation on magnetohydrodynamics nanofluid flow and heat transfer by means of two phase model, J. Magn. Magn. Mater. 374 (2014) 36–43.
[44] M. Sheikholeslami, M. Gorji Bandpy, R. Ellahi, M. Hassan, S. Soleimani, Effects of MHD on Cu–water nanofluid flow and heat transfer by means of CVFEM, J. Magn. Magn. Mater. 349 (2014) 188–200.
[45] M.S. Valipour, S. Rashidi, M. Bovand, R. Masoodi, Numerical modeling of flow around and through a porous cylinder with diamond cross section, Eur. J. Mech. B/Fluids 46 (2014) 74–81.
[46] M.S. Valipour, S. Rashidi, R. Masoodi, Magnetohydrodynamics flow and heat transfer around a solid cylinder wrapped with a porous ring, ASME J. Heat Transf. 136 (2014) 062601–062609. http://dx.doi.org/10.1115/1.4026371.
[47] M.S. Valipour, R. Masoodi, S. Rashidi, M. Bovand, M. Mirhosseini, A numerical study of convection around a square porous cylinder using Al_2O_3–H_2O nanofluid, Therm. Sci. 18 (4) (2014) 1305–1314.
[48] A. Weickgenannt, P.A. Monkewitz, Control of vortex shedding in an axisymmetric bluff body wake, Eur. J. Mech. B/Fluids 19 (2000) 789–812.
[49] F.M. White, Fluid Mechanics, 6th ed., McGraw Hill Book Company, New York, 2009.
[50] H.S. Yoon, H.H. Chun, M.Y. Ha, H.G. Lee, A numerical study on the fluid flow and heat transfer around a circular cylinder in an aligned magnetic field, Int. J. Heat Mass Transf. 47 (2004) 4075–4087.
[51] M. Zhao, L. Cheng, B. Teng, D. Liang, Numerical simulation of viscous flow past two circular cylinders of different diameters, Appl. Ocean Res. 27 (1) (2005) 39–55.